DOI 10.1016/j.ica.2020.119567

Unusual monodentate binding of a *C*-NONOate ligand in the nitrosyl complex (OEP)Ru(NO)(η^1-ONN(*t*-Bu)O)

Nan Xu,[a]* Alexander Bevak,[a] Joseph Roesch,[a] Bernadette Armstrong,[a] Erwin Abucayon,[b] Zachary Bell,[a] Douglas R. Powell,[b] and George B. Richter-Addo[b]*

[a] Department of Chemistry, Pennsylvania State University, Altoona College, 3000 Ivyside Park, Altoona, Pennsylvania, U.S.A., 16601. Email: nxx103@psu.edu

[b] Department of Chemistry and Biochemistry, University of Oklahoma, 101 Stephenson Parkway SLSRC, Norman, Oklahoma, U.S.A., 73019. Email: grichteraddo@ou.edu

Abstract

The recent discovery of the *C*-NONOate moiety ($[X\{N_2O_2\}]^-$; diazeniumdiolate) as a new class of siderophore functional group necessitates further examination of its coordination chemistry. The bidentate η^2-*O*,*O* binding mode of the *C*-NONOate moiety is well-established. We have synthesized and characterized, by X-ray crystallography, the first monodentate η^1-O binding mode of a *C*-NONOate group to any metal, namely that of (OEP)Ru(NO)(η^1-ONN(*t*-Bu)O). The compound exhibits an irreversible first oxidation in CH_2Cl_2 at a Pt electrode. Protonation with triflic acid results in the formation of N_2O, presumably from the direct protonation of the *C*-NONOate ligand.

1. Introduction

Nitric oxide (NO) [1, 2] and its organic derivatives [3, 4] display varied coordination chemistries that help shed light on their biological functions. An important class of NO derivatives are the NONOates ($[X\{N_2O_2\}]^-$; diazeniumdiolates) that contain two NO groups linked to an organic X fragment (Figure 1) [5]. The most commonly studied NONOates are the *C*-NONOates (X = carbon-linked) and *N*-NONOates (X = nitrogen-linked), although others are known as well.

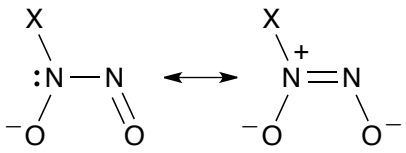

Figure 1. Sketch of the NONOate functional group.

The coordination chemistry of the *C*-NONOate group has attracted renewed attention due to the recent discovery of naturally occurring *C*-NONOates whose functions are metal-dependent. Such naturally occurring *C*-NONOates include the anticancer and antiviral agent alanosine isolated from *Streptomyces alanocinicus* (Figure 2) [6-8]; its biosynthetic pathway, including examination of the gene-cluster responsible for the $–N_2O_2$ installation, was recently elucidated [9].

Of particular interest, however, is the recent discovery of a new class of bacterial siderophores in the rhizosphere whose metal-binding units comprise *C*-NONOate functional groups. This discovery presents a major advance in the siderophore field, where the *C*-NONOate

moiety now joins the well-established siderophore classes of catecholates, hydroxamates, and α-hydroxycarboxylates [10]. Gramibactin (Figure 2), isolated from the plant-associated bacterium

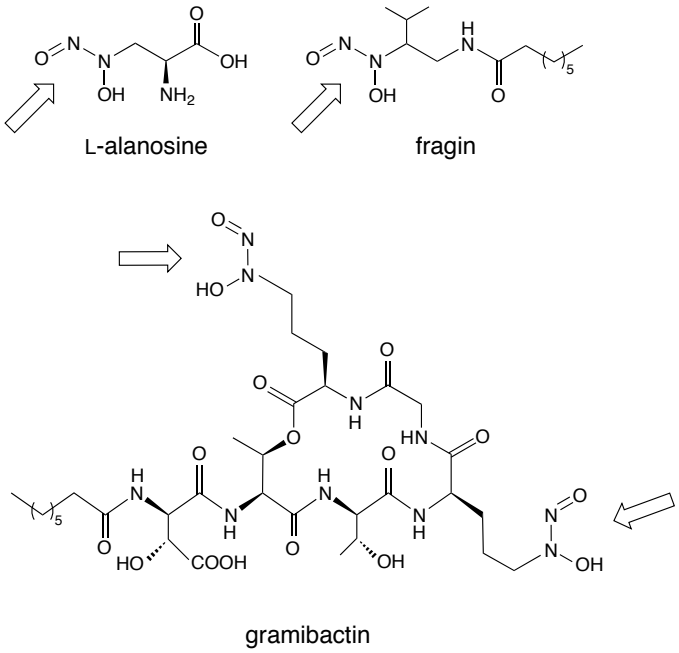

Figure 2. Chemical structures of selected naturally occurring *C*-NONOate compounds.

P. graminis, was the first *C*-NONOate-based siderophore to be discovered (in 2018) [11], and it showed Fe-binding efficiencies comparable to those of hydroxamate-based siderophores. Importantly, the ability of gramibactin to release NO presented a secondary capability of its metal-dependent siderophore function. Additional *C*-NONOate based siderophores such as megapolibactin, plantaribactin, and gladiobaction have since been discovered [12]. Other naturally occurring *C*-NONOates include the antiviral agent fragin (Figure 2) [5, 13], dopastin [5], the cell-to-cell signaling molecule valdiazen [13], and the free-radical scavenger peocillanosine [14].

In terms of the coordination chemistry of *C*-NONOates, the established binding mode is the bidentate η^2-*O*,*O* mode, where both O-atoms of the $[X\{N_2O_2\}]^-$ moiety (Figure 1) directly

coordinate the metal center. Such bidentate binding has provided an important baseline for our understanding of *C*-NONOate action. However, it has remained unclear if an optional and stable monodentate binding mode of the *C*-NONOate moiety is possible, as it had never been reported. We reported the preparation of *C*-NONOate adducts of Fe heme models [15, 16], and these displayed the bidentate mode of the *C*-NONOate ligands. Given the fact that siderophores bind metals, we further explored the fundamental coordination chemistry of *C*-NONOates with metalloporphyrins to probe the formation of both η^2-*O*,*O* and η^1-*O* binding modes. In this paper, we report the successful generation and properties of the first structurally characterized η^1-*O* binding mode in a *C*-NONOate complex of any metal.

2. Experimental

2.1. General

The reactions were performed under an anaerobic (nitrogen) atmosphere using standard Schlenk glassware and/or in a dry box. Cyclohexane and CH_2Cl_2 were distilled from CaH_2 under nitrogen just prior to use. The precursor alkoxide (OEP)Ru(NO)(O-*i*-C_5H_{11}) was synthesized from the *trans*-addition reaction of (OEP)Ru(CO) with isoamyl nitrite as described previously [17]. The *N*-*t*-butyl-*N*-nitrosohydroxylamine HON(*t*-Bu)NO reagent and its ^{15}N-labeled analog were prepared by literature methods [18].

2.2. Instrumentation

General characterization methods were similar to those described previously [19-22]. Namely, electrochemical measurements were performed using a BAS CV-50W instrument. For cyclic voltammetry, a three-electrode cell with a 3 mm diameter Pt disk working electrode, a Pt

wire counter electrode, and a Ag/AgCl reference electrode were utilized. The solutions for all electrochemical experiments were 1.0 mM in analyte, in 10 mL CH_2Cl_2 solution containing 0.1M NBu_4PF_6 as support electrolyte. The solutions were deaerated by purging with prepurified nitrogen for 10 min before each set of measurements, and then the nitrogen atmosphere was maintained during the measurements which were performed at room temperature (~20 °C).

Infrared spectra for the synthetic work were collected on Bio–Rad FT–155 (at OU) and a Nicolet iS10 FTIR (at UPA) spectrometers. For infrared spectroelectrochemistry, the experimental setup consisted on the same cell utilized for the cyclic voltammetry measurements, with the 3 mm Pt disk working electrode serving as the mirror for the fiber optic mid-IR dip probe, as described previously [19, 20, 23]. The resulting IR spectra were recorded using a Bruker Vector 22 FTIR spectrometer equipped with a liquid nitrogen cooled MCT detector (Remspec Corporation, Sturbridge, MA, USA). ^{1}H NMR spectra were collected on a Varian 400 MHz NMR spectrometer.

2.3 Synthesis

(OEP)Ru(NO)(η^1-ONN(*t*-Bu)O). To a CH_2Cl_2 (15 mL) solution of (OEP)Ru(NO)(OC_5H_{11}) (28.6 mg, 0.038 mmol) under an atmosphere of nitrogen was added a CH_2Cl_2 solution of a large excess of *N*-*t*-butyl-*N*-nitrosohydroxylamine. The solution was stirred at room temperature overnight, during which time the color of the solution gradually changed from red to brown-red. The solution was reduced to ~3 mL in vacuo and 25 mL cyclohexane was added to result in dark purple precipitate. The light purple supernatant was removed by filtration, and the residue dried in vacuo to give (OEP)Ru(NO)(η^1-ONN(*t*-Bu)O) (18.0 mg, 0.023 mmol, 61% isolated yield). IR (KBr, cm^{-1}): υ_{NO} 1814 s; $\upsilon_{ONN(O)}$ 1427 m, 1068 m, 972 m. ^{1}H NMR ($CDCl_3$;

400 MHz, ppm): 10.34 (s, *meso*-H of OEP), 4.17 (app q, J = ~8 Hz, 16H, CH_2CH_3 of OEP), 2.02 (t, J = 8 Hz, 24H, CH_2CH_3 of OEP), –0.26 (s, 9H, $-C(CH_3)_3$ of axial NONOate ligand). Isolated product yields typically ranged from 54–72%, although the reaction in solution went to full conversion as judged by IR spectroscopy.

Single crystals of (OEP)Ru(NO)(η^1-ONN(*t*-Bu)O) suitable for X-ray crystallography were obtained from the slow evaporation of a CH_2Cl_2/cyclohexane solution of the compound at room temperature.

Protonation of (OEP)Ru(NO)(η^1-ONN(*t*-Bu)O) to generate N_2O: Triflic acid (8.54 μL, 0.097 mmol) was added dropwise to a stirred CH_2Cl_2 (5.0 mL) solution of (OEP)Ru(NO)(η^1-ONN(*t*-Bu)O) (21.2 mg, 0.0242 mmol) in a sealed Schlenk tube at room temperature. The brown-red solution immediately began to change color to a darker brown. The reaction mixture was stirred for overnight. An IR spectrum of a sample of the reaction headspace (transferred via gas-tight syringe into a gas IR cell) revealed bands at 2236/2213 cm^{-1} indicative of N_2O formation. The IR bands obtained when ^{15}N-labeled (OEP)Ru(NO)(η^1-O^{15}NN(*t*-Bu)O) was used showed formation of the singly-labeled $^{14}N^{15}NO$ (υ_{asym} 2190/2169 cm^{-1}, with a minor band at 2212 cm^{-1}) [24]. The IR spectrum of the residual solid after solvent evaporation from the product mixture showed a band at 1854 cm^{-1} (NaCl plate) assigned to the υ_{NO} of the cationic $[(OEP)Ru(NO)(H_2O)]^+$ [25] byproduct of the reaction formed in the presence of trace moisture.

2.4 X-ray crystallography

A red prism-shaped crystal of dimensions 0.17 x 0.38 x 0.61 mm was selected for structural analysis. Intensity data for this compound were collected using a diffractometer with a Bruker APEX ccd area detector [26, 27] and graphite-monochromated Mo Kα radiation (λ =

0.71073 Å). The sample was cooled to 100(2) K. Cell parameters were determined from a non-linear least squares fit of 12151 peaks in the range $2.3 < \theta < 28.3°$. A total of 43241 data were measured in the range $1.596 < \theta < 28.363°$ using ϕ and ω oscillation frames. The data were corrected for absorption by the semi-empirical method [28] giving minimum and maximum transmission factors of 0.794 and 0.936. The data were merged to form a set of 19981 independent data with R(int) = 0.0507 and a coverage of 100.0 %.

The monoclinic space group *C*2/*m* was determined by systematic absences and statistical tests and verified by subsequent refinement. The structure was solved by direct methods and refined by full-matrix least-squares methods on F^2 [29, 30]. Hydrogen atom positions were initially determined by geometry and refined using a riding model. Non-hydrogen atoms were refined with anisotropic displacement parameters. Hydrogen atom displacement parameters were set to 1.2 (1.5 for methyl) times the isotropic equivalent displacement parameters of the bonded atoms. A total of 249 parameters were refined against 19981 data to give $wR(F^2)$ = 0.1302 and S = 1.003 for weights of $w = 1/[\sigma^2(F^2)+ (0.0580\ P)^2 + 3.8500\ P]$, where $P = [F_o^2 + 2F_c^2] / 3$. The final R(*F*) was 0.0556 for the 16246 observed, $[F > 4\sigma(F)]$, data.

The selected crystal was a two-component non-merohedral twin. A cyclohexane molecule was severely disordered and was best modeled using the program *Squeeze* [31]. The metal complex was located on a mirror plane, so only half of the atoms were unique. Crystal data and structural refinement parameters are shown in Table 1. CCDC 1964627 contains the supplementary crystallographic data. These data can be obtained free of charge via www.ccdc.cam.ac.uk/data_request/cif, or by emailing data_request@ccdc.cam.ac.uk, or by contacting The Cambridge Crystallographic Data Centre, 12, Union Road, Cambridge CB2 1EZ, UK; fax: +44 1223 336033.

Table 1. Crystal Data and Structure Refinement

Empirical formula (f.w.)	$C_{40}H_{53}N_7O_3Ru$ (780.96)
Crystal system	monoclinic
Space group	*C2/m*
Unit cell dimensions	
a (Å)	22.0467(19)
b (Å)	15.6792(13)
c (Å)	12.9306(11)
b (°)	99.403(2)
Z, Z′	4, 0.5
F(000)	1640
Absorption coefficient	0.396 mm^{-1}
Max. and min. transmission	0.936 and 0.794
Theta range for data collection (°)	1.596-28.363
Reflections collected	43241
Independent reflections	19981 [R(int) = 0.0507]
Data / restraints / parameters	19981 / 0 / 249
wR(F^2 all data)[a]	*wR2* = 0.1302
R(*F* obsd data)[b]	R1 = 0.0556
Goodness-of-fit on F^2	1.003
Observed data [$I > 2\sigma(I)$]	16246
Largest mean mean shift / s.u.	0.001 and 0.000
Largest diff. peak and hole (e/$Å^3$)	1.017 and –0.647

[a] $wR2 = \{\Sigma[w(F_o^2 - F_c^2)^2] / \Sigma[w(F_o^2)^2]\}^{1/2}$. [b] $R1 = \Sigma||F_o| - |F_c|| / \Sigma|F_o|$.

3. Results and discussion

3.1 Preparation and spectroscopy

The desired (OEP)Ru(NO)(η^1-ONN(*t*-Bu)O) product was obtained by the reaction of excess *N*-*t*-butyl-*N*-nitrosohydroxylamine HON(*t*-Bu)NO with the precursor alkoxide (OEP)Ru(NO)(O-*i*-C_5H_{11}) in CH_2Cl_2 (eq. 1). The reaction was monitored by IR spectroscopy

$$(OEP)Ru(NO)(OC_5H_{11}) + HON(t\text{-}Bu)NO \rightarrow (OEP)Ru(NO)(\eta^1\text{-}ONN(t\text{-}Bu)O) + HOC_5H_{11} \quad (1)$$

and was essentially complete over a ~12 h period, where the υ_{NO} band of the precursor alkoxide (at 1800 cm^{-1}; CH_2Cl_2) was gradually replaced by the υ_{NO} band of the product (at 1838 cm^{-1}; CH_2Cl_2). The target dark purple (OEP)Ru(NO)(η^1-ONN(*t*-Bu)O) product was isolated in 54–72% yields after workup.

The IR spectrum of (OEP)Ru(NO)(η^1-ONN(*t*-Bu)O) shows a strong υ_{NO} band at 1814 cm^{-1} (KBr pellet; Figure 3) which is 24 cm^{-1} higher than that of the precursor (OEP)Ru(NO)(O-*i*-C_5H_{11}) (1790 cm^{-1}; KBr pellet) indicative of the axial η^1-ONN(*t*-Bu)O ligand being an overall weaker electron donor than the precursor isoamyl alkoxide. Three ^{15}N-isotope sensitive bands at 1427 cm^{-1}, 1068 cm^{-1} and 972 cm^{-1} are associated with the ligand; these bands shift to

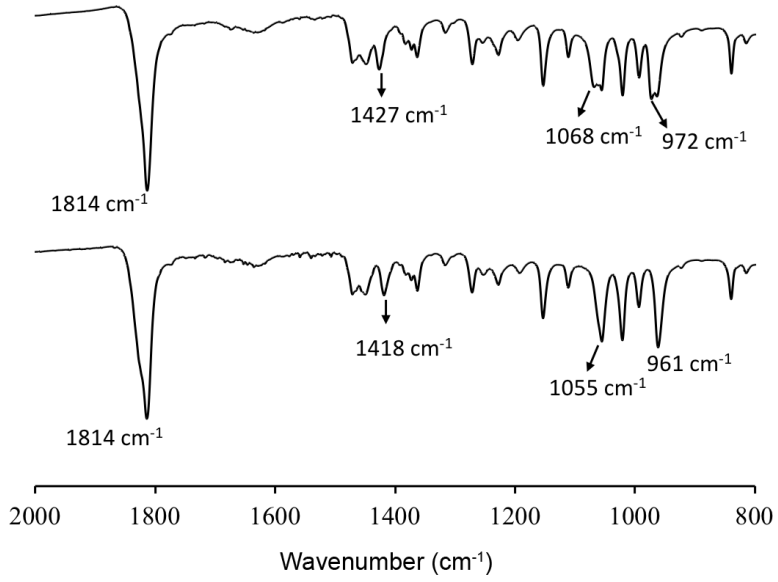

Figure 3. IR spectra of (OEP)Ru(NO)(η^1-ONN(*t*-Bu)O) (*top*) and the ^{15}N-labeled (OEP)Ru(NO)(η^1-O^{15}NN(*t*-Bu)O) (*bottom*) as KBr pellets.

1418 cm^{-1}, ~1055 cm^{-1} and ~ 961 cm^{-1} respectively, with the latter two overlapping with the porphyrin bands (bottom of Figure 3).

The ^{1}H-NMR spectrum of (OEP)Ru(NO)(η^1-ONN(*t*-Bu)O) in $CDCl_3$ shows, in addition to the characteristic peaks for the OEP macrocycle, a single peak at –0.26 ppm assigned to the –C(CH_3)$_3$ group of the axial NONOate ligand. Similar upfield shifts for axial ligands due to the porphyrin ring current have been observed in other nitrosyl ruthenium porphyrin complexes [22].

3.2 Crystallography

The crystal structure of (OEP)Ru(NO)(η^1-ONN(*t*-Bu)O) is shown in Figure 4 with selected bond lengths and angles displayed on the left of Figure 5.

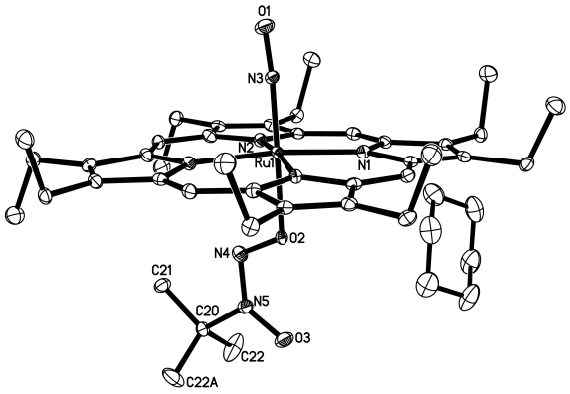

Figure 4. Molecular structure of (OEP)Ru(NO)(η^1-ONN(*t*-Bu)O) as a cyclohexane solvate. Hydrogen atoms have been omitted for clarity.

The nitrosyl RuNO moiety is linear with a ∠RuNO of 173.9(3)°, with Ru–N and N–O distances of 1.740(4) Å and 1.156(5) Å, respectively. The linearity of the RuNO linkage is consistent with those observed for most, but not all, neutral {RuNO}^{6} nitrosyl porphyrin complexes [2, 32]. Notable exceptions include the nitrosyl compounds with a strong σ-donor aryl/alkyl ligands

(por)Ru(NO)(*p*-C_6H_4F) (por = TTP [33], OEP [34]) and (T(*p*-OMe)PP)Ru(NO)Et [22] where the ∠RuNO angles are ~152–155°. The equatorial Ru–N(por) bond lengths are 2.055(3)-2.056(3) Å and are unremarkable for this class of compounds.

The most interesting feature of the structure is the observed monodentate *O*-binding mode of the ONN(*t*-Bu)O ligand to the ruthenium center with an axial Ru–O bond length of 2.026(3) Å.

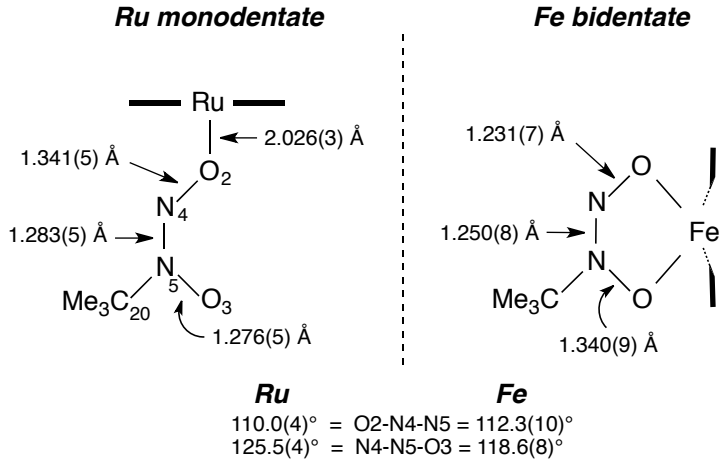

Figure 5. Selected geometrical parameters for the metal-NONOate axial cores in (*Left*) the monodentate (OEP)Ru(NO)(η^1-ONN(*t*-Bu)O) (this work) and (*Right*) the previously reported bidentate (OEP)Fe(η^2-ONN(*t*-Bu)O).

The N4–O2 and N5–O3 bond lengths in (OEP)Ru(NO)(η^1-ONN(*t*-Bu)O) are dissimilar at 1.341(5) Å and 1.276(5) Å, respectively (left of Figure 5). Curiously, and although we do not have a Ru bidentate NONOate compound to compare these data to, this trend is opposite to that observed in the six-coordinate bidentate compound (OEP)Fe(η^2-ONN(*t*-Bu)O) (right of Figure 5; identical porphyrin and NONOate groups) where the N–O distance in the group adjacent to the *t*-Bu group is longer than that for the other N–O group. The ∠O2–N4–N5 and ∠N4–N5–O3 angles are also dissimilar at 110.0(4)° and 125.5(4)°, with a difference (Δ of ~16°) much larger

than that observed, not surprisingly, for the bidentate mode of this NONOate ligand in the related six-coordinate Fe complex (Δ of ~6°; right of Figure 5).

Importantly, however, this structure of (OEP)Ru(NO)(η^1-ONN(*t*-Bu)O) represents the first example of a complex containing a monodentate *C*-NONOate. A copper complex containing a monodentate *N*-NONOate ligand $[Et_2N(N_2O_2)]^-$ has been reported [35], but this latter compound is also the sole example of such a binding mode for the *N*-NONOate class of compounds.

3.3 Protonation to generate N_2O

We previously reported that the bidentate *C*-NONOate ligand in (OEP)Fe(η^2-ONN(*t*-Bu)O) undergoes protonation by triflic acid to generate N_2O [15]. We were interested in determining if a similar reaction was possible with our target monodentate compound (OEP)Ru(NO)(η^1-ONN(*t*-Bu)O). Protonation with ~4 equiv of triflic acid did, indeed, generate N_2O (υ_{asym} 2236/2213 cm^{-1}) identified by gas-phase IR spectroscopy. The use of the ^{15}N-labeled (OEP)Ru(NO)(η^1-O^{15}NN(*t*-Bu)O) analog resulted in the generation of $^{14}N^{15}NO$ (2190/2169 cm^{-1} identified by its characteristic IR spectral data [24]. The generation of this mixed isotope $^{14}N^{15}NO$ suggests that protonation does not involve an initial cleavage of the N–N bond upon protonation, which would yield an isolated and unstable "H^{15}NO" intermediate that would dimerize [36] to yield exclusively $^{15}N_2O$. An alternative mechanism would need to be considered, for example one that involves protonation at either –O^{15}N<u>*N*</u>(*t*-Bu)<u>*O*</u> site. Further studies are in progress to determine the pathway operative in this protonation reaction.

3.4 Redox behavior and IR spectroelectrochemistry

The redox behavior of (OEP)Ru(NO)(η^1-ONN(*t*-Bu)O) in CH_2Cl_2 at a Pt electrode was examined by electrochemistry and infrared spectroelectrochemistry at room temperature (~19 °C). The cyclic voltammogram is shown in Figure 6, and reveals an irreversible first oxidation with E_{pa} of +0.61 V (referenced to the ferrocene/ferrocinium couple), and a reversible second oxidation with $E^{o\prime}$ of +0.73 V. The first oxidation remains irreversible when the scan is reversed just after the first oxidation, and the two weak reduction peaks are the daughter peaks due to this irreversible first oxidation. These two latter cathodic peaks (at negative potentials) are not present when the reduction scan was performed first. We are unable to assign these cathodic peaks to specific redox products at this time due to limited data available. Additional work will involve isolation of the oxidation products and independently probing their redox/reduction behaviors as controls. We note that peak intensity for the second oxidation is larger at slower scan rates (e.g., larger at 100 mV/s versus at 1 V/s), suggesting that it results from the

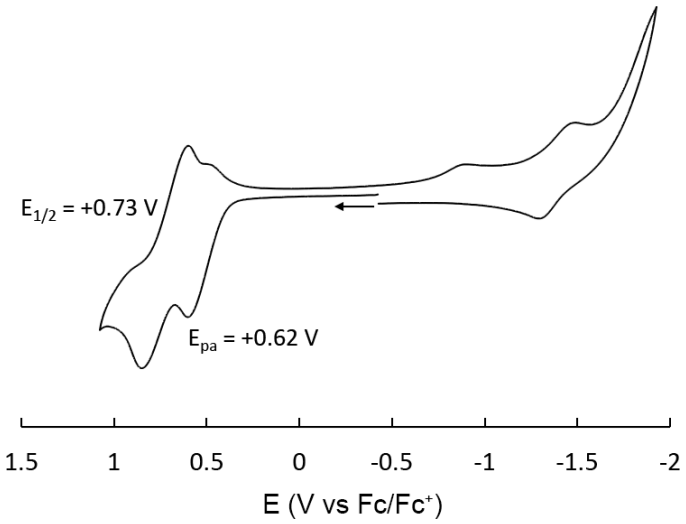

Figure 6. Cyclic voltammogram of (OEP)Ru(NO)(η^2-ONN(*t*-Bu)O) in CH_2Cl_2 containing 0.1 M NBu_4PF_6 at room temperature (scan rate of 200 mV/s).

decomposition of the first oxidation product. We also note that the redox potential of $[(OEP)Ru(NO)(H_2O)]BF_4$ in a near-identical solvent system has been reported to be at +0.71 V (see later).

To probe the identity of the products from the oxidations, we performed IR spectroelectrochemical measurements using our procedures described previously. The resulting difference IR spectra are shown in Figure 7. When the potential is held just past that for the first oxidation, a new IR band is observed at 1876 cm^{-1} (in CH_2Cl_2) assigned to υ_{NO}, which is close to those of $[(OEP)Ru(NO)(L)]^+$-type compounds (L = H_2O (1877 cm^{-1}) or py (1876 cm^{-1})) [37], indicating rapid loss of the *trans*-axial ligand (trans to axial NO). However, when the IR spectral data is collected using shorter timescales (e.g., 20 scans vs. 72 scans), this first oxidation indicates the transient formation of an 1860 cm^{-1} band prior to its conversion to that associated with the υ_{NO} of the $[(OEP)Ru(NO)(L)]^+$ product at 1876 cm^{-1}. We thus assign this 1860 cm^{-1}

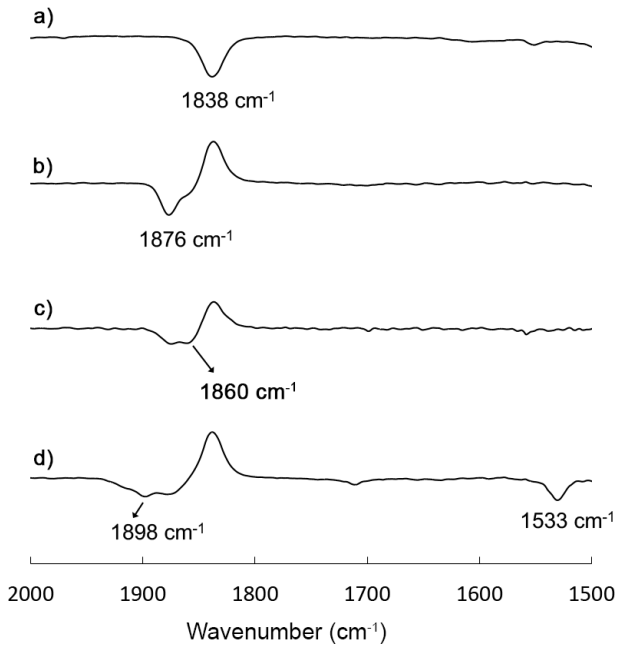

Figure 7. Difference FTIR spectra showing the υ_{NO}s of the compounds before the oxidation (a), and during the 1st oxidation (b), 1st oxidation (fast; c), and the second oxidation (d).

band to the υ_{NO} of the initial oxidized derivative [(OEP)Ru(NO)(η^1-ONN(*t*-Bu)O)]$^+$ that forms prior to its decomposition. Based on the redox behaviors of other (por)Ru(NO)X derivatives, we presume that the initial site of oxidation is initially the porphyrin ring, as this will be consistent with the low $\Delta\upsilon_{NO}$ of +22 cm^{-1} for this oxidation that occurs somewhat distant from the axial moiety. We note that valence isomerizations (i.e., porphyrin oxidation vs ligand oxidation) are not uncommon in metalloporphyrin chemistry [38]. When the applied potential is held just past the second oxidation, a new υ_{NO} band at 1898 cm^{-1} is observed which is similar to that of the electrogenerated dicationic compound [(OEP$^{\bullet}$)Ru(NO)(H_2O)]$^{2+}$ (1895 cm^{-1}) [37] containing a π-radical cationic porphyrin. Indeed, the new band at 1533 cm^{-1} (bottom trace in Figure 7) is consistent with the formation of a stable OEP-based π-radical cation [39]. Consequently, we conclude that the first oxidation of (OEP)Ru(NO)(η^1-ONN(*t*-Bu)O) results in the net dissociation of the NONOate ligand forming the monocationic [(OEP)Ru(NO)(L)]$^+$ (L = solvent or H_2O) species, whereas the reversible second oxidation is due to the oxidation of this electrogenerated monocation.

4. Conclusion

In this work, we have characterized the first monodentate η^1-O binding mode of a *C*-NONOate ligand in a metal complex, namely (OEP)Ru(NO)(η^1-ONN(*t*-Bu)O). This compound was sufficiently stable in solution at room temperature to allow for its isolation, crystallization, and structure solution by X-ray crystallography. The observed net irreversible chemical oxidation results in the loss of the axial *C*-NONOate group to generate the [(OEP)Ru(NO)(L)]$^+$ derivative. Protonation of the compound with triflic acid to yield N_2O suggests a potentially rich chemistry of the coordinated *C*-NONOate group. This type of protonation chemistry is important

to unravel, as *C*-NONOates are known to be bona fide siderophore functional groups that can be metabolized to yield inorganic NO_x fragments. Further studies are currently underway to explore the reactivity of the coordinated *C*-NONOate group.

Acknowledgements

We are grateful to Penn State University Altoona for support (to NX), and to the National Science Foundation (CHE-1900181 and CHE-1566509 to GBRA) for funding for this research.

References

[1] G.B. Richter-Addo, P. Legzdins, Metal Nitrosyls, Oxford University Press, New York, 1992.

[2] L. Cheng, G.B. Richter-Addo, Binding and Activation of Nitric Oxide by Metalloporphyrins and Heme, in *The Porphyrin Handbook*; R. Guilard, K. Smith, K.M. Kadish (Eds.), Academic Press, New York, 2000, Volume 4, Chapter 33, pp. 219-291.

[3] N. Xu, G.B. Richter-Addo, Interactions of Nitrosoalkanes/arenes, Nitrosamines, Nitrosothiols, and Alkyl Nitrites with Metals, Prog. Inorg. Chem., 59 (2014) 381-445.

[4] J. Lee, L. Chen, A.H. West, G.B. Richter-Addo, Interactions of Organic Nitroso Compounds with Metals, Chem. Rev., 102 (2002) 1019-1065.

[5] J.A. Hrabie, L.K. Keefer, Chemistry of the Nitric Oxide-Releasing Diazeniumdiolate ("Nitrosohydroxylamine") Functional Group and Its Oxygen-Substituted Derivatives, Chem. Rev., 102 (2002) 1135-1154.

[6] H.N. Jayaram, A.K. Tyagi, S. Anandaraj, J.A. Montgomery, J.A. Kelley, J. Kelley, R.H. Adamson, D.A. Cooney, Metabolites of Alanosine, an Anti-Tumor Antibiotic, Biochem. Pharmacol., 28 (1979) 3551-3566.

[7] Y.K.S. Murthy, J.E. Thiemann, Coronell.C, P. Sensi, Alanosine a New Antiviral and Antitumour Agent Isolated from a *Streptomyces*, Nature, 211 (1966) 1198-1199.

[8] G. Powis, J.S. Kovach, Binding of Copper and Zinc by the Anti-Tumor Agent L-Alanosine, Biochem Pharmacol, 30 (1981) 771-776.

[9] T.L. Ng, M.E. McCallum, C.R. Zheng, J.X. Wang, K.J.Y. Wu, E.P. Balskus, The L-Alanosine Gene Cluster Encodes a Pathway for Diazeniumdiolate Biosynthesis, ChemBioChem, (2019) Epub ahead of print. DOI: 10.1002/cbic.201900565.

[10] E.A. Dertz, K.N. Raymond, Siderophores and Transferrins, Comp. Coord. Chem. II, Elsevier, New York, 2003, Chapter 8.6, pp. 141-168.

[11] R. Hermenau, K. Ishida, S. Gama, B. Hoffmann, M. Pfeifer-Leeg, W. Plass, J.F. Mohr, T. Wichard, H.P. Saluz, C. Hertweck, Gramibactin is a Bacterial Siderophore with a Diazeniumdiolate Ligand System, Nat Chem Biol, 14 (2018) 841-843.

[12] R. Hermenau, J.L. Mehl, K. Ishida, B. Dose, S.I. Pidot, T.P. Stinear, C. Hertweck, Genomics-Driven Discovery of NO-Donating Diazeniumdiolate Siderophores in Diverse Plant-Associated Bacteria, Angew Chem Int Edit, 58 (2019) 13024-13029.

[13] C. Jenul, S. Sieber, C. Daeppen, A. Mathew, M. Lardi, G. Pessi, D. Hoepfner, M. Neuburger, A. Linden, K. Gademann, L. Eberl, Biosynthesis of Fragin is Controlled by a Novel Quorum Sensing Signal, Nat Commun, 9 (2018).

[14] T. Natori, Y. Kataoka, S. Kato, H. Kawai, N. Fusetani, Poecillanosine, A New Free Radical Scavenger from the Marine Sponge *Poecillastra spec aff tenuilaminaris*, Tetrahedron Lett, 38 (1997) 8349-8350.

[15] N. Xu, J.H. Christian, N.S. Dalal, E.G. Abucayon, C. Lingafelt, D.R. Powell, G.B. Richter-Addo, Six-Coordinate Ferric Porphyrins Containing Bidentate *N*-*t*-butyl-*N*-

Nitrosohydroxylaminato Ligands: Structure, Magnetism, IR Spectroelectrochemisty, and Reactivity, Dalton Trans., 44 (2015) 20121-20130.

[16] G.-B. Yi, M.A. Khan, G.B. Richter-Addo, Metalloporphyrins with $X[N_2O_2]^-$ Ligands. Novel High-Spin (*N*-Phenyl-*N*-nitrosohydroxylaminato)(*meso*-tetraarylporphyrinato)iron(III), Inorg. Chem., 34 (1995) 5703-5704.

[17] G.-B. Yi, L. Chen, M.A. Khan, G.B. Richter-Addo, Activation of Thionitrites and Isoamyl Nitrite by Group 8 Metalloporphyrins and the Subsequent Generation of Nitrosyl Thiolates and Alkoxides of Ruthenium and Osmium Porphyrins, Inorg. Chem., 36 (1997) 3876-3885.

[18] N. Arulsamy, D.S. Bohle, J.A. Imonigie, E.S. Sagan, Correlation of the Product E/Z Framework Geometry and O-O vs O-N Regioselectivity in the Dialkylation of Hyponitrite, J. Am. Chem. Soc., 122 (2000) 5539-5549.

[19] M.J. Shaw, R.L. Henson, S.E. Houk, J.W. Westhoff, M.W. Jones, G.B. Richter-Addo, Fiber-Optic Infrared Reflectance Spectroelectrochemistry: Isomerization of a Manganese Pyranyl Complex, J. Electroanal. Chem., 534 (2002) 47-53.

[20] S.M. Carter, J. Lee, C.A. Hixson, D.R. Powell, R.A. Wheeler, M.J. Shaw, G.B. Richter-Addo, Fiber-Optic Infrared Reflectance Spectroelectrochemical Studies of Osmium and Ruthenium Nitrosyl Porphyrins Containing Alkoxide and Thiolate Ligands, Dalton Trans., (2006) 1338-1346.

[21] N. Xu, A.W. Bevak, B.R. Armstrong, D.R. Powell, Synthesis, Characterization and Solid State Molecular Structures of Five- And Six-Coordinate Primary Amide Manganese Porphyrin Complexes, Polyhedron, 127 (2017) 432-437.

[22] N. Xu, J. Lilly, D.R. Powell, G.B. Richter-Addo, Synthesis, Characterization, and Infrared Reflectance Spectroelectrochemistry of Organoruthenium Nitrosyl Porphyrins, Organometallics, 31 (2012) 827-834.

[23] Z.N. Zahran, M.J. Shaw, M.A. Khan, G.B. Richter-Addo, Fiber-Optic Spectroelectrochemical Studies of Six-Coordinate Manganese Nitrosyl Porphyrins in Nonaqueous Media, Inorg. Chem., 45 (2006) 2661-2668.

[24] Y. Dubowski, D. Harush, A. Shaviv, L. Stone, R. Linker, Real Time Monitoring of N_2O Emissions from Agricultural Soils using FTIR Spectroscopy, Soil Sci. Soc. Am. J., 78 (2014) 61-69.

[25] G.-B. Yi, M.A. Khan, G.B. Richter-Addo, Ruthenium Porphyrins Containing Nitrosyl, Nitrosamine, Thiolate, and Amine Ligands, Inorg. Chem., 35 (1996) 3453-3454.

[26] APEX2, Data Collection: APEX2 Software Reference Manual, Bruker-AXS, Madison, WI, 2007.

[27] SAINT, SAINT: Data Reduction and Correction Program, Data Reduction: SAINT Software Reference Manual. Bruker-AXS, Madison, WI. , (2007).

[28] L. Krause, R. Herbst-Irmer, G.M. Sheldrick, D. Stalke, Comparison of Silver and Molybdenum Microfocus X-Ray Sources for Single-Crystal Structure Determination, J. Appl. Cryst., 48 (2015) 3-10.

[29] G.M. Sheldrick, *SHELXT* - Integrated Space-Group and Crystal-Structure Determination, Acta Cryst., A71 (2015) 3-8.

[30] G.M. Sheldrick, Crystal Structure Refinement with *SHELXL*, Acta Cryst., C71 (2015) 3-8.

[31] A.L. Spek, PLATON SQUEEZE: a Tool for the Calculation of the Disordered Solvent Contribution to the Calculated Structure Factors, Acta Cryst. , C71 (2015) 9-18.

[32] N. Xu, J. Lee, D.R. Powell, G.B. Richter-Addo, Synthesis, Characterization, and Redox Behavior of Six-Coordinate (por)Ru(NO)Cl Compounds (por = porphyrinato dianion), Inorg. Chim. Acta, 358 (2005) 2855-2860.

[33] S.J. Hodge, L.-S. Wang, M.A. Khan, V.G. Young, Jr., G.B. Richter-Addo, The First Structurally Characterized Organometallic Nitrosyl Porphyrin: Structure of [Ru(ttp)(NO)(C_6H_4F-*p*)(ttp = meso-tetratolylporphyrinato dianion), Chem. Commun., (1996) 2283-2284.

[34] G.B. Richter-Addo, R.A. Wheeler, C.A. Hixon, L. Chen, M.A. Khan, M.K. Ellison, C.E. Schulz, W.R. Scheidt, Unexpected Nitrosyl Group Bending in Six-Coordinate $\{MNO\}^6$ σ-Bonded Aryl(iron) and -Ruthenium Porphyrins, J. Am. Chem. Soc., 123 (2001) 6314-6326.

[35] J.L. Schneider, J.A. Halfen, V.G. Young, W.B. Tolman, Mono- versus Bidentate Coordination of the NONOate $[Et_2N(N_2O_2)]^-$ to Copper(II) Complexes of Tetradentate Ligands, New J. Chem., 22 (1998) 459-466.

[36] J.M. Fukuto, M.D. Bartberger, A.S. Dutton, N. Paolocci, D.A. Wink, K.N. Houk, The Physiological Chemistry and Biological Activity of Nitroxyl (HNO): The Neglected, Misunderstood, and Enigmatic Nitrogen Oxide, Chem. Res. Toxicol., 18 (2005) 790-801.

[37] P. Singh, A.K. Das, B. Sarkar, M. Niemeyer, F. Roncaroli, J.A. Olabe, J. Fiedler, S. Zalis, W. Kaim, Redox Properties of Ruthenium Nitrosyl Porphyrin Complexes with Different Axial Ligation: Structural, Spectroelectrochemical (IR, UV-visible, and EPR), and Theoretical Studies, Inorg. Chem., 47 (2008) 7106-7113.

[38] S. Ozawa, H. Fujii, I. Morishima, NMR Studies of Iron(II) Nitrosyl π-Cation Radicals of Octaethylchlorin and Octaethylisobacteriochlorin as Models for Reaction Intermediate of Nitrite Reductase, J. Am. Chem. Soc., 114 (1992) 1548-1554.

[39] E.T. Shimomura, M.A. Phillippi, H.M. Goff, W.F. Scholz, C.A. Reed, Infrared Spectroscopy of Oxidized Metalloporphyrins: Detection of a Band Diagnostic of Porphyrin-Centered Oxidation, J. Am. Chem. Soc., 103 (1981) 6778-6780.

Supporting Information

Unusual monodentate binding of a *C*-NONOate ligand in the nitrosyl complex (OEP)Ru(NO)(η^1-ONN(*t*-Bu)O)

Nan Xu, Alexander Bevak, Joseph Roesch, Bernadette Armstrong, Erwin Abucayon, Zachary Bell, Douglas R. Powell, and George B. Richter-Addo

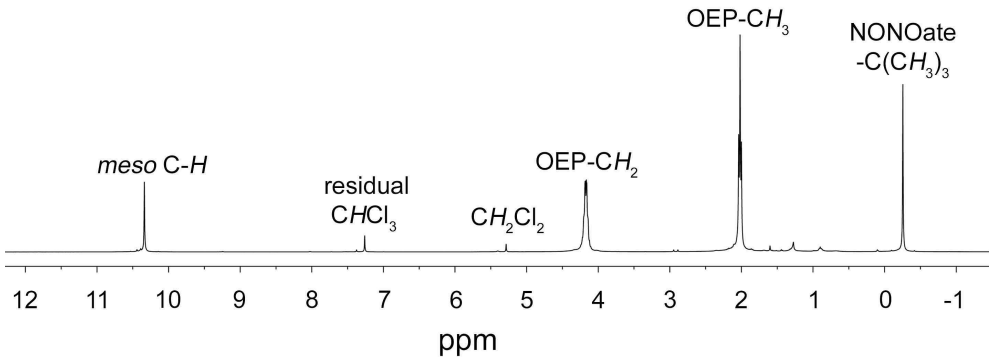

Figure S1. 400 MHz ^{1}H NMR spectrum of (OEP)Ru(NO)(η^1-ONN(*t*-Bu)O) in $CDCl_3$. [see Experimental Section in the main text for details].